

# DFT/TDDFT Study of Lanthanide<sup>III</sup> Mono- and Bisporphyrin Complexes

Meng-Sheng Liao, John D. Watts, and Ming-Ju Huang\*

Department of Chemistry, P. O. Box 17910, Jackson State University, Jackson, Mississippi 39217

Received: May 25, 2006; In Final Form: September 27, 2006

The electronic structure, molecular structure, and electronic spectra of lanthanide<sup>III</sup> mono- and bisporphyrin complexes are investigated using a DFT/TDDFT method. These complexes include YbP(acac), YbP<sub>2</sub>, [YbP<sub>2</sub>]<sup>+</sup>, YbHP<sub>2</sub>, and [YbP<sub>2</sub>]<sup>-</sup> (where P = porphine and acac = acetylacetonate). To shed some light on the origin of the out-of-plane displacement of Yb in YbP(acac), unligated model systems, namely, planar *D*<sub>4h</sub> and distorted *C*<sub>4v</sub> YbP, were calculated. For comparison, the calculations were also extended to include the Ce<sup>IV</sup>P<sub>2</sub> and [Ce<sup>IV</sup>P<sub>2</sub>]<sup>+</sup> systems. Even without an axial ligand, the lanthanide atom lies considerably above the porphyrin plane; the distortion of the YbP molecular structure from a planar *D*<sub>4h</sub> to the nonplanar *C*<sub>4v</sub> symmetry leads to a considerable energy lowering. The axial ligand makes the metal out-of-plane displacement even larger, and it also changes the redox properties of the lanthanide monoporphyrin. The ground-state configurations of YbP<sub>2</sub> and YbHP<sub>2</sub> were determined by considering several possible low-lying states. YbP<sub>2</sub> is confirmed to be a single-hole radical. The special redox properties of the bisporphyrin complexes can well be accounted for by the calculated ionization potentials and electron affinities. The TDDFT results provide a clear description of the UV–vis and near-IR absorption spectra of the various lanthanide porphyrins.

## 1. Introduction

Metal porphyrins (MPors) have been the subject of intense research because of their great biological importance and the unique nature of their coordination chemistry. (Here, we use Por to refer to any porphyrin.) While experimental studies of MPors have been expanded by the synthesis and characterization of species containing heavy metals, lanthanides, and actinides, theoretical studies have mainly been devoted to the first-row transition metal porphyrins. The combination of lanthanides (Ln) with porphyrins results in two different classes of interesting complexes: the lanthanide monoporphyrinates<sup>1a</sup> and the lanthanide “sandwich” bisporphyrinates.<sup>1b</sup> Since the lanthanides are too large to fit into the constrained porphyrin core, a large out-of-plane displacement of the metal in lanthanide porphyrins has been observed. Lanthanide monoporphyrins always exist in the form of LnPor(L)<sub>*n*</sub>, where L is an axial ligand; they have been studied as luminescent centers in near-infrared (IR) polymer electroluminescent devices,<sup>2–5</sup> photochemical probes,<sup>6,7</sup> NMR dipolar probe and shift reagents,<sup>8–10</sup> contrast agents,<sup>11</sup> as well as electroactive materials for ion-sensitive electrodes.<sup>12</sup> Iwase and Igarashi reported electrochemical behaviors of a series of LnTPP(acac) complexes.<sup>13</sup>

In lanthanide bisporphyrins Ln(Por)<sub>2</sub>, the Ln atom holds two macrocycles close together. Strong electronic interactions between the porphyrins in the stacked porphyrins impart unique properties to these systems. Complexes of this type are proving to be useful as structural models of the photosynthetic reaction center in bacteria, and they possess spectroscopic and electrochemical properties similar to those of the special pair of *Rhodospseudomonas viridis*.<sup>14,15</sup> As a result, there have been many experimental studies of the M(Por)<sub>2</sub> compounds in recent years.<sup>16–25</sup> They are also of interest because of their electrochromic, semiconducting, and nonlinear optical properties.<sup>26</sup> In comparison to analogous monoporphyrins, there are two notable

features of M(Por)<sub>2</sub>: a blue-shift of the B (or Soret) bands and a decrease in the oxidation potential.<sup>16,17</sup> In addition, the porphyrin sandwich compounds have a number of characteristic optical properties that are not exhibited by monoporphyrins or dimers having larger spacing between the rings. For example, Ln<sup>III</sup>(Por)<sub>2</sub> or the  $\pi$ -radical cations, [M<sup>IV</sup>(Por)<sub>2</sub>]<sup>+</sup> (formed by oxidation), exhibit an intense broad band in the near-IR region (1000–1400 nm)<sup>20,22</sup> not found in simple MPor or [MPor]<sup>+</sup>. This near-IR absorption was proposed to arise from an electronic transition between the porphyrin–porphyrin bonding and antibonding orbitals.<sup>20</sup> Buchler and Scharbert measured optical spectra of the whole series of compounds Ln(OEP)<sub>2</sub> (Ln = La–Lu).<sup>22</sup>

Theoretical investigations on lanthanide porphyrins are very rare. A recent calculation on the cerium bisporphine, CeP<sub>2</sub>, was reported by Ricciardi et al.<sup>27</sup> The electronic structure of CeP<sub>2</sub> is relatively simple with a closed-shell ground state, where the oxidation state of Ce is +4. For other lanthanide bisporphyrins, however, the oxidation state of Ln is +3. In this case, the ground state is, in essence, a ring  $\rightarrow$  metal charge transfer (CT) state; one electron has been transferred from the porphyrin ring(s) to the metal to form a neutral complex. Different from the closed-shell Ce<sup>IV</sup>(Por)<sub>2</sub> species, Ln<sup>III</sup>(Por)<sub>2</sub> contains a single hole in the porphyrin  $\pi$  system. A notable characteristic of the single-hole species is a near-IR absorption band.<sup>20,22</sup> The electronic structures of the Ln<sup>III</sup>(Por)<sub>2</sub> complexes have not been explored in detail. To our knowledge, no theoretical studies of LnPor(L)<sub>*n*</sub> have been performed so far.

This paper comprises a density functional theory/time-dependent density functional theory (DFT/TDDFT) study of the YbP(acac), YbP<sub>2</sub>, YbHP<sub>2</sub>, and [YbP<sub>2</sub>]<sup>-</sup> complexes, where P stands for the simple porphine and acac designates the bidentate ligand, acetylacetonate. The molecular structures of the complexes are illustrated in Figure 1. They share the common feature that the lanthanide atom sits above the porphyrin plane. Normal transition metal porphyrins are planar (Figure 1a). The Pors used

\* Corresponding author. E-mail: mhuang@chem.jsums.edu.

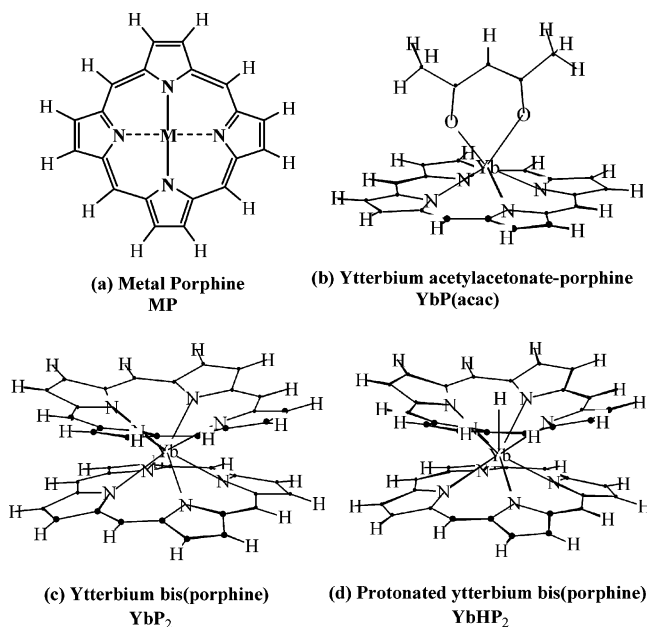


**Figure 1.** Molecular structures of MP, YbP(acac), YbP<sub>2</sub>, and YbHP<sub>2</sub>.

in the experiments were tetraphenylporphine (TPP) and octaethylporphine (OEP). Previous calculations<sup>28</sup> have shown that the smaller P is able to mimic the essential properties of the more complicated species.

Spyroulias and co-workers<sup>29–32</sup> also reported synthesis and (optical and electrochemical) characterization of protonated forms of double-deckers, namely, LnH(Por)<sub>2</sub> for Ln = Nd–Lu, where the H atom was suggested to reside atop one of the porphyrin rings.<sup>31</sup> For the asymmetrical complexes, one group of the four pyrrole nitrogens is not equal to another. In a basic solvent such as DMF or pyridine, the proton is abstracted, leading to a deprotonated form [Ln(Por)]<sup>−</sup>.<sup>29</sup> To examine the influence of the axial hydrogen on the properties of the double-deckers, our calculations were extended to include the YbHP<sub>2</sub> and [YbP<sub>2</sub>]<sup>−</sup> systems. In addition, to see the difference between Ln<sup>III</sup>(Por)<sub>2</sub> and Ce<sup>IV</sup>(Por)<sub>2</sub>, results for CeP<sub>2</sub> and [CeP]<sup>+</sup> were also presented.

The main aim of this work is two-fold: (i) To provide a detailed description of the ground-state electronic structures of the mentioned ytterbium porphyrin complexes and their precise structural information. Accurate structural parameters for LnPor(acac) are unknown although the NMR spectra confirm the formation of paramagnetic metal porphyrins with the metal considerably displaced from the porphyrin plane. (ii) To provide a quantitative interpretation for the spectral properties of the systems.

## 2. Computational Details

All calculations were carried out using the Amsterdam density functional (ADF) program package ADF2005.01.<sup>33–36</sup> The STO basis set employed is the standard ADF-TZP, which is triple- $\zeta$  for valence orbitals plus one polarization function. To obtain accurate results, the valence set on the lanthanides included subvalence 5s and 5p shells. For N, C, and O, 2s and 2p were considered as valence shells. The other shells of lower energy, i.e., [Kr]4d<sup>10</sup> for Yb/Ce and [He] for N/C/O, were described as core and kept frozen according to the frozen-core approximation.<sup>33</sup> Among the various exchange-correlation potentials available, the density-parametrization form of Vosko, Wilk, and Nusair (VWN)<sup>37</sup> plus Becke's gradient correction for exchange (B)<sup>38</sup> and Perdew's gradient correction for correlation (P)<sup>39</sup> were

employed. It has been shown that the combined VWN-B-P functional can give accurate bonding energies for both main group<sup>40</sup> and transition metal<sup>41</sup> systems. Relativistic corrections of the valence electrons were calculated by the quasi-relativistic (QR) method.<sup>42</sup> (The relativistic corrections of atomic cores are taken into account at the Dirac–Fock level.) In this scalar (one-component) approach, spin–orbit (SO) coupling is not taken into account. Because SO effects are mainly atomic in nature, they are not expected to have significant influence on molecular properties<sup>43</sup> except metal–ligand binding energies.<sup>44</sup> Calculations on open-shell systems were performed using the spin-unrestricted method.

Electron excitation energies related to the electronic absorption spectra were calculated using the time-dependent density functional response theory (TDDFT)<sup>45</sup> as implemented in the ADF program. TDDFT provides a first-principles method for the calculation of excitation energies and presents an excellent alternative to the conventional highly correlated configuration interaction (CI) method. The recent implementation of TDDFT in the updated ADF program allows calculations of excitation energies for open-shell systems.

The ionization potentials (IPs) and electron affinities (EAs) were calculated by the so-called  $\Delta$ SCF method in which separate SCF calculations for the neutral molecule and its ion are carried out and  $IP = E(X^+) - E(X)$  and  $EA = E(X^-) - E(X)$ . The ionized and reduced species were reoptimized, but they are shown to undergo little geometry change as compared to the neutral species (see Table 3).

As mentioned in the Introduction, one aim of the present work is to provide precise structural information on ytterbium porphyrin complexes. Actually, the molecular structure of each system studied here has been optimized in order to obtain the “correct” electronic structure and energetic properties. The geometry optimization was done within certain symmetry specified for the system, and the choice of the symmetry is based on the most probable geometries of the molecule and the available X-ray crystal structures of comparable compounds. As the present model porphyrins are highly symmetric and rigid, the geometry optimization can be expected to converge to a minimum. The good agreement between the calculated and available experimental bond lengths and angles supports this point of view.

## 3. Results and Discussion

**3.1. Electronic Structure, Structural, and Energetic Properties.** **3.1.1. YbP(acac).** For comparison, we also calculated two model systems of unligated YbP, which are in square planar  $D_{4h}$  and distorted  $C_{4v}$  symmetries, respectively. Figure 2 illustrates the changes of electronic structure from YbP ( $D_{4h}$ ) to YbP ( $C_{4v}$ ) to YbP(acac) ( $C_{2v}$ ). With a 4f<sup>10</sup>6s<sup>2</sup> configuration for Yb, the ground state of YbP is a closed-shell state. The highest occupied molecular orbitals (HOMOs) are a set of 4f orbitals. As pointed out in the Introduction, lanthanides do not form in-plane complexes with (normal) porphyrins, which may be attributed to a poor match between the atomic size and the macrocycle cavity diameter. In planar YbP (YbP- $D_{4h}$ ), the relatively small core size of P results in a large  $\sigma$ -donor interaction that elevates the lanthanide 4f orbitals greatly so that they lie considerably above the porphyrin  $a_{2u}$  orbital. When the central metal moves out of the plane, the  $\sigma$ -donor interaction is reduced and the 4f orbitals are shifted down. When YbP is ligated by acac, the axial ligand abstracts an electron from the 4f orbitals, and so the 4f orbitals are further lowered and now located around the porphyrin  $a_{2u}$  and  $a_{1u}$  orbitals in YbP(acac).

**TABLE 1: Calculated Properties of Ytterbium Monoporphyrin Complexes<sup>a</sup>**

	YbP ( $D_{4h}$ )	YbP ( $C_{4v}$ )	Yb(acac)	YbP(acac) ( $C_{2v}$ )	
				calc	exptl
$R_{Yb-N}$ , Å	2.204	2.264		2.321	2.326 <sup>c</sup>
$R_{Ct(N4)\cdots N}$ , Å <sup>b</sup>		2.089		2.076	2.055 <sup>c</sup>
$R_{Ct(N4)\cdots Yb}$ , Å		0.874		1.037	1.090 <sup>c</sup>
$R_{Ct(N4)\cdots Ct(C8)}$ , Å <sup>b</sup>		0.228		0.141	
$R_{Ct(N4)\cdots Ct(H8)}$ , Å <sup>b</sup>		0.328		0.201	
$R_{Yb-O}$ , Å			2.167	2.251	2.22 <sup>d</sup>
$\angle OYbO$ , deg			82.4	75.4	73.4 <sup>d</sup>
Yb-5d, e	0.74	0.77	0.43	0.91	
Yb-4f, e	13.73	13.60	13.74	13.29	
$Q_{Yb}$	1.68	1.67	0.65	1.94	
$E_{bind}(Yb-P)$ , eV	8.08	9.65		8.70 <sup>e</sup>	
IP, eV		6.27 (1e/f-like)		6.62 (28a <sub>1</sub> )	
		6.74 (a <sub>1</sub> )		7.35 (20b <sub>2</sub> /f-like)	
EA, eV		-1.26 (2e)		-2.21 (24b <sub>1</sub> /f-like)	
				-1.05 (25b <sub>1</sub> )	

<sup>a</sup>  $R$ , distance;  $\angle$ , angle; Ln-5d/4f, Mulliken orbital population;  $Q$ , atomic charge;  $E_{bind}$ , binding energy; IP, ionization potential; EA, electron affinity. <sup>b</sup>  $Ct(N4)$ , centroid of the plane defined by the four pyrrole nitrogen atoms;  $Ct(C8)$ , centroid of the plane defined by the eight peripheral carbon atoms;  $Ct(H8)$ , centroid of the plane defined by the eight peripheral hydrogen atoms. <sup>c</sup> X-ray crystal structure data on YbTPP(H<sub>2</sub>O)(THF)(Cl) (ref 46). <sup>d</sup> Estimated from crystallographic results on lanthanide  $\beta$ -diketonate complexes (ref 9). <sup>e</sup> This binding energy is defined as  $-E_{bind} = E[YbP(acac)] - E[Yb(acac)] - E(P)$ .

**TABLE 2: Calculated Relative Energies ( $E$ , eV) for Selected Configurations in YbP<sub>2</sub>, CeP<sub>2</sub>, and YbHP<sub>2</sub>**

system	configuration <sup>a</sup>	term	$E_{relative}$	oxidation state on Ln
YbP <sub>2</sub>	$(12b_2/f)^1(11a_1)^2(5a_2)^1(15e_3/f)^4$	<sup>3</sup> B <sub>1</sub>	0	Yb <sup>III</sup>
	$(12b_2/f)^2(11a_1)^2(5a_2)^1(15e_3/f)^3$	<sup>3</sup> E <sub>3</sub> (A)	0.57	Yb <sup>III</sup>
	$(12b_2/f)^1(11a_1)^2(5a_2)^2(15e_3/f)^3$	<sup>3</sup> E <sub>3</sub> (B)	0.77	Yb <sup>IV</sup>
	$(12b_2/f)^2(11a_1)^2(5a_2)^0(15e_3/f)^4$	<sup>1</sup> A <sub>1</sub>	0.89	Yb <sup>II</sup>
	$(12b_2/f)^2(11a_1)^1(5a_2)^1(15e_3/f)^4$	<sup>3</sup> A <sub>2</sub>	0.91	Yb <sup>II</sup>
CeP <sub>2</sub>	$(5a_2)^2$	<sup>1</sup> A <sub>1</sub>	0	Ce <sup>IV</sup>
	$(5a_2)^1(15e_3)^1$	<sup>3</sup> E <sub>3</sub>	1.15	Ce <sup>III</sup>
YbHP <sub>2</sub>	$(15b_2)^1(15b_1)^2(31e)^4(23a_1)^2(10a_2)^2$	<sup>2</sup> B <sub>2</sub>	0	Yb <sup>III</sup>
	$(15b_2)^2(15b_1)^1(31e)^4(23a_1)^2(10a_2)^2$	<sup>2</sup> B <sub>1</sub>	0.13	Yb <sup>III</sup>
	$(15b_2)^2(15b_1)^2(31e)^3(23a_1)^2(10a_2)^2$	<sup>2</sup> E	0.19	Yb <sup>III</sup>
	$(15b_2)^2(15b_1)^2(31e)^4(23a_1)^2(10a_2)^1$	<sup>2</sup> A <sub>2</sub>	0.43	Yb <sup>II</sup>
	$(15b_2)^2(15b_1)^2(31e)^4(23a_1)^1(10a_2)^2$	<sup>2</sup> A <sub>1</sub>	0.56	Yb <sup>II</sup>

<sup>a</sup> See Figure 4 for the orbitals; here “f” means an f-like orbital.

The degeneracy of the f orbitals is split with a bandwidth of  $\sim 0.2$  eV. Although the axial ligand acac lowers the symmetry of YbP from  $C_{4v}$  to  $C_{2v}$ , no split is found between the 2e-derived orbitals, 25b<sub>1</sub> and 21b<sub>2</sub>.

Table 1 presents the calculated properties for YbP- $D_{4h}$ , YbP- $C_{4v}$ , Yb(acac), and YbP(acac); they include various structural parameters ( $R$ ,  $\angle$ ), Mulliken orbital populations (Yb-5d, Yb-4f), Mulliken atomic charge ( $Q$ ), Yb-P binding energies ( $E_{bind}$ ), ionization potentials (IP), and electron affinities (EA).  $E_{bind}$  is defined as

$$-E_{bind} = E(YbP) - \{E(Yb) + E(P)\}$$

where  $E(YbP)$ ,  $E(Yb)$ , and  $E(P)$  are the total energies of the indicated species. (The  $E_{bind}$  is not corrected with the zero-point energy, which is expected to be small for the relatively large systems. That is, the vibration frequency of the Yb-P bond is expected to be low as both Yb and P are relatively large moieties.)  $R_{Ct(N4)\cdots N}$  is a measure of the porphyrin core size and  $R_{Ct(N4)\cdots Yb}$  represents the displacement of the metal out of the porphyrin plane.

The  $E_{bind}$  values indicate that distorted YbP- $C_{4v}$  is  $\sim 1.6$  eV more stable than planar YbP- $D_{4h}$ , owing primarily to the energy lowering of the HOMOs. The displacement of Yb above the plane defined by the four pyrrole N atoms is as large as

0.87 Å. Figure 3 illustrates the change of the relative energy of YbP with the motion of the metal out of the plane. (At each fixed  $R$ , the structure of YbP was reoptimized under  $C_{4v}$  symmetry.) The potential curve shows the Yb atom has a strong tendency to move out of the porphyrin plane.  $R_{Ct(N4)\cdots Yb}$  increases by  $\sim 0.16$  Å when YbP is attached by acac. There are X-ray crystal structure data available for YbTPP(H<sub>2</sub>O)(THF)(Cl), wherein Yb is displaced by 1.090 Å,<sup>46</sup> in good agreement with the calculation (1.04 Å). On the other hand, the calculated Yb-O distance (2.25 Å) and OYbO angle (75.4°) in YbP(acac) agree well with those (2.22 Å, 73.4°) estimated from crystallographic results on lanthanide  $\beta$ -diketonate complexes.<sup>9</sup> We also calculated the fragment system Yb(acac); it is shown that both the distance and angle change significantly on going from Yb(acac) to YbP(acac).

The gross Yb-5d population in YbP- $C_{4v}$  is  $\sim 0.8$  e, showing a large electron donation from the ring ligand lone pair to the metal ion; on the other hand, there is about 0.4 e back-donation from the metal 4f orbitals to the ring, with the result that the positive charge on Yb in YbP- $C_{4v}$  is  $\sim 1.7$  e.  $Q_{Yb}$  is increased by only  $\sim 0.3$  e from Yb<sup>III</sup>P to Yb<sup>III</sup>P(acac).

The Yb-P binding energy in YbP- $C_{4v}$  is estimated to be 9.7 eV. With the presence of acac, the Yb-P bond is destabilized by about 1 eV, owing to the strong binding between Yb and acac.

The first ionization of YbP- $C_{4v}$  occurs from a high-lying f orbital. In the case of YbP(acac), the energies of the f orbitals are greatly lowered, and so the first ionization now takes place from the porphyrin  $a_{2u}$  (28a<sub>1</sub>), in agreement with electrochemical results that the center of oxidation of LnPor(acac) is on the porphyrin base.<sup>13</sup> The calculated first IP of YbP(acac) is  $\sim 0.4$  eV larger than that of YbP, suggesting that the axial ligation makes the oxidation of the system more difficult. This ligation also changes the electron affinity and the character of the LUMO (lowest unoccupied MO). For YbP, the added electron goes into the high-lying, antibonding porphyrin 2e orbitals. In contrast, the added electron in YbP(acac) now occupies a low-lying f orbital. Therefore, the EA of YbP(acac) is more than 1 eV higher than that of YbP.

3.1.2. YbP<sub>2</sub>. Ln(Por)<sub>2</sub> is a sandwich-like complex in which the macrocycle rings are staggered by about 45° (Figure 1c). This symmetry has been well established by experiment, and

**TABLE 3: Calculated Properties of Lanthanide Bisporphyrin Complexes at the Ground State<sup>a</sup>**

	Yb <sup>III</sup> P <sub>2</sub>	Ce <sup>IV</sup> P <sub>2</sub>		[Yb <sup>III</sup> P <sub>2</sub> ] <sup>+</sup>	[Ce <sup>IV</sup> P <sub>2</sub> ] <sup>+</sup>	Yb <sup>III</sup> HP <sub>2</sub>	[Yb <sup>III</sup> P <sub>2</sub> ] <sup>-</sup>
		calc	exptl <sup>b</sup>				
$\Delta E(D_{4d} - D_{4h})$ , eV	-0.20	-0.38		-0.09	-0.28	-0.50	-0.44
$R_{Ln-N}$ , Å	2.476	2.526	2.475	2.462	2.522	2.556, 2.409 <sup>c</sup>	2.503
$R_{Ct(N4)\cdots N}$ , Å <sup>d</sup>	2.060	2.077	2.057	2.055	2.079	2.029, 2.063	2.070
$R_{Ct(N4)\cdots Ln}$ , Å	1.374	1.438	1.376	1.357	1.428	1.554, 1.244	1.407
$R_{Ct(N4)\cdots Ct(C8)}$ , Å <sup>d</sup>	0.512	0.532		0.522	0.506	0.617, 0.526	0.540
$R_{Ct(N4)\cdots Ct(H8)}$ , Å <sup>d</sup>	0.726	0.762		0.747	0.728	0.868, 0.728	0.763
$R_{P-P}$ , Å <sup>e</sup>	2.748	2.876	2.752	2.714	2.856	2.798	2.814
$R_{Ct(N4)\cdots H(ax)}$ , Å						0.594	
$R_{N-H(ax)}$ , Å						2.114	
Ln-5d, e	0.89	1.27		0.92	1.26	0.99	0.80
Ln-4f, e	13.36	0.88		13.36	0.90	13.30	13.37
$Q_{Ln}$	2.06	2.01		2.08	2.01	2.06	2.04
$E_{bind}(Ln-2P)$ , eV	14.09	19.30		14.34 <sup>f</sup>	19.00 <sup>f</sup>	15.04 <sup>g</sup>	18.80 <sup>h</sup>
IP, eV	6.02 (5a <sub>2</sub> )	6.17 (5a <sub>2</sub> )				6.09 (10a <sub>2</sub> )	
	6.11 (11a <sub>1</sub> )	6.30 (11a <sub>1</sub> )				6.30 (23a <sub>1</sub> )	
	6.38 (15e <sub>2</sub> /f) <sup>i</sup>					7.28 (31e <sub>1</sub> /f)	
	6.54 (16e <sub>1</sub> /f)						
	6.66 (15e <sub>3</sub> /f)						
EA, eV	-2.98 (5a <sub>2</sub> )	-2.12 (15e <sub>3</sub> /f)				-2.54 (15b <sub>2</sub> /f)	
	-2.28 (12b <sub>2</sub> /f)	-1.23 (16e <sub>3</sub> )					

<sup>a</sup> See the legend of Table 1. <sup>b</sup> X-ray crystal structure data on Ce(OEP)<sub>2</sub> (ref 25). <sup>c</sup> The second set of values represents the structural parameters related to the other, lower-part, porphyrin ring which does not carry an axial H atom (see Figure 1d). <sup>d</sup> See the legend of Table 1. <sup>e</sup>  $R_{P-P}$ , which is equal to  $2R_{Ct(N4)\cdots Ln}$ , represents the distance between two porphyrins in the dimer. <sup>f</sup> The value of the binding energy for the positive ion is defined as  $-E_{bind} = E([LnP_2]^+) - E(Ln^+) - 2E(P)$ . <sup>g</sup> Here  $-E_{bind} = E(YbHP_2) - E(Yb) - 2E(P) - E(H)$ . <sup>h</sup> Here  $-E_{bind} = E([YbP_2]^-) - E(Yb^-) - 2E(P)$ . <sup>i</sup> Here "f" means an f-like orbital.

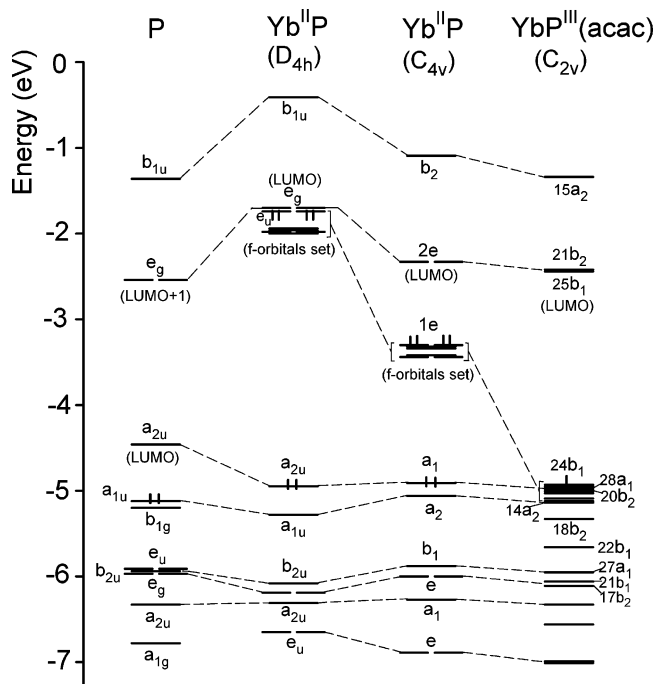


**Figure 2.** Orbital energy levels for the valence orbitals of P, YbP- $D_{4h}$ , YbP- $C_{4v}$ , and YbP(acac).

our calculations show that the square antiprismatic  $D_{4d}$  conformation is indeed preferred over a face-to-face conformation which maintains  $D_{4h}$  symmetry (see Table 3). Another structural feature of Ln(Por)<sub>2</sub> is that both porphyrins are domed and severely distorted from planarity. This is also confirmed by the calculations. The saucer-like deformation of the macrocycle is necessary to improve the overlap of the porphyrin pair and to maximize the Ln-N interaction.

To determine the ground state for YbP<sub>2</sub>, the energetics of several possible low-lying states were computed, whose relative energies are presented in Table 2. (Geometry optimization was performed for all states. The same is true for other molecules

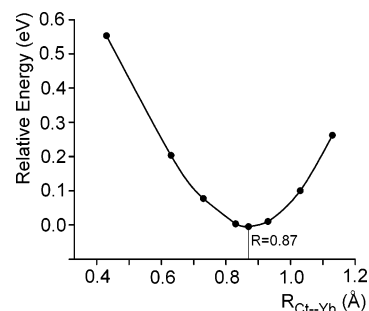


**Figure 3.** Variation of the relative energy of YbP with the Yb out-of-plane displacement.

listed in Table 2.) According to the results, the lowest energy electronic configuration for YbP<sub>2</sub> is clearly  $(12b_2/f)^1(5a_2)^1$ , where one electron is located in a Yb-4f orbital and the other resides in a P<sub>2</sub> orbital. There seem to be no other competing low-lying states. Figure 4 illustrates the P, P<sub>2</sub>, and YbP<sub>2</sub> orbital energy levels and their correlations. The P<sub>2</sub> MOs are formed from linear combination of the P MOs of appropriate symmetry; they are split into bonding and antibonding pairs. Interaction of the P HOMOs ( $a_{1u}$ ) leads to a large splitting and the bonding and antibonding MOs are  $b_1$  and  $a_2$ , respectively. The two lowest unoccupied MOs (LUMOs) ( $a_{2u}$ ) of P overlap to form the  $b_2$  and  $a_1$  orbitals, which split relatively weakly. In P<sub>2</sub>,  $b_2$  and  $a_2$  become the HOMO and LUMO, respectively. For the higher-lying virtual orbitals of P<sub>2</sub>,  $2e_3$  and  $2e_1$  are the bonding and antibonding MOs of the  $e_g^*$  orbitals of monoporphyrins.

Since in YbP<sub>2</sub> the 5a<sub>2</sub> orbital is occupied by only one electron, the trivalent lanthanide sandwich complex contains a single hole in the P<sub>2</sub>  $\pi$ -system, and this hole is apparently delocalized through the P-P interaction. Therefore, there is net bonding interaction in the ground state of YbP<sub>2</sub>. Under  $D_{4d}$  symmetry, the metal 4f orbitals transform as  $b_2$ ,  $e_1$ ,  $e_2$ , and  $e_3$  and they are split widely. There are no metal f orbitals of appropriate symmetry to mix with the HOMO 5a<sub>2</sub>.

The orbital energy level diagram of CeP<sub>2</sub> is presented on the right-hand side in Figure 4. In this bisporphyrin, seven unoc-



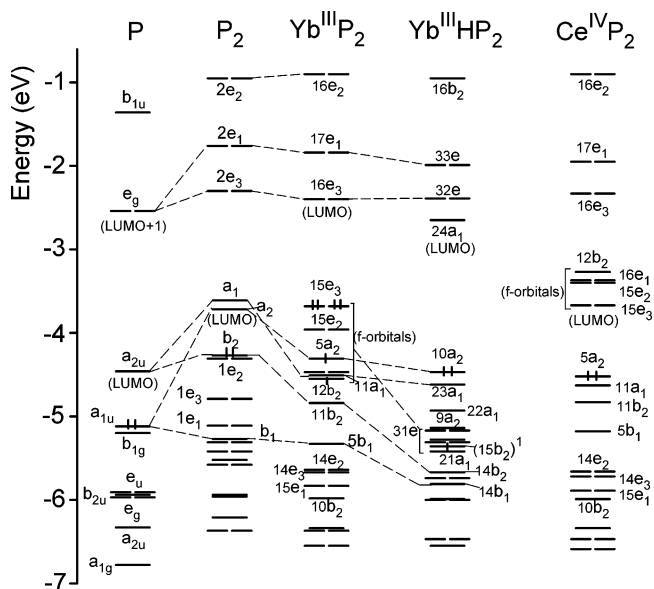


**Figure 4.** Orbital energy levels for the valence orbitals of P, P<sub>2</sub>, YbP<sub>2</sub>, YbHP<sub>2</sub>, and CeP<sub>2</sub>.

cupied 4f-like orbitals (15e<sub>3</sub>, 15e<sub>2</sub>, 16e<sub>1</sub>, 12b<sub>2</sub>) all lie well above the 5a<sub>2</sub> orbital and they constitute the LUMOs. The ground state of CeP<sub>2</sub> is clearly (5a<sub>2</sub>)<sup>2</sup>, a closed-shell <sup>1</sup>A<sub>1</sub> state. There is no single electron that occupies a 4f orbital, and so Ce in CeP<sub>2</sub> has the oxidation state of +4.

The calculated properties of ground-state YbP<sub>2</sub> are presented in Table 3, together with the results of CeP<sub>2</sub> for comparison. Here  $E_{\text{bind}}$  is defined as

$$-E_{\text{bind}} = E(\text{LnP}_2) - \{E(\text{Ln}) + 2E(\text{P})\}$$

which provides one measure of the extent of  $\pi$ - $\pi$  overlap interaction in LnP<sub>2</sub>. As mentioned above, the porphyrin in LnP<sub>2</sub> adopts a domed conformation.  $R_{\text{Ct}(\text{N}4)\cdots\text{Ct}(\text{H}8)}$  is a direct measure of the doming in such complexes. We also presented in the table the distance between the N4 and C8 planes,  $R_{\text{Ct}(\text{N}4)\cdots\text{Ct}(\text{C}8)}$ .

The Yb atom in YbP<sub>2</sub> sits 1.37 Å above the centroid of the plane defined by the four pyrrole N atoms. This is larger than the displacement of the metal in YbP(acac) (1.04 Å). The doming defined by  $R_{\text{Ct}(\text{N}4)\cdots\text{Ct}(\text{H}8)}$  is as large as 0.73 Å. In Table 3,  $R_{\text{P-P}}$  represents the P-P distance, which is taken as the distance between the planes defined by the four N atoms of each ring. According to this definition, the two macrocycles in YbP<sub>2</sub> are separated by 2.75 Å. The total height of the molecule as measured from one H8 plane to another H8 plane is 4.2 Å. As Ce<sup>IV</sup> is bigger than Yb<sup>III</sup> (1.01 vs 0.94 Å), the calculated structural parameters for CeP<sub>2</sub> are all slightly larger than those for YbP<sub>2</sub>; even the doming is larger in CeP<sub>2</sub> than in YbP<sub>2</sub>. There are X-ray crystal structure data available for the OEP substituted sandwich Ce(OEP)<sub>2</sub>,<sup>25</sup> which are in good agreement with the calculation.

The Ln-P<sub>2</sub> binding energy is large, 14.1 eV for YbP<sub>2</sub> and 19.3 eV for CeP<sub>2</sub>. This accounts for the high stability of the Ln(Por)<sub>2</sub> complexes.

According to the calculation, the first ionization occurs from the 5a<sub>2</sub> orbital. Thus, one-electron oxidation of Yb(Por)<sub>2</sub> will produce a double-hole [Yb(Por)<sub>2</sub>]<sup>+</sup> species. The second hole resides in the same MO as the first hole, consistent with a resonance Raman (RR) spectroscopy study.<sup>19</sup> Electron spin resonance (ESR) spectra recorded for the two-hole complexes also suggested no unpaired electrons reside in the porphyrin  $\pi$ - $\pi$  system at room or low temperature.<sup>19</sup> As sandwich

porphyrin cations have been the subject of experimental studies,<sup>18,19,22</sup> Table 3 also reports the optimized structural parameters for [YbP<sub>2</sub>]<sup>+</sup>, which indicate that the positive ion is slightly ‘tighter’ than the neutral species because removal of an electron from the antibonding dimer MO would increase the net  $\pi$ - $\pi$  bond order in the ground state. Owing to the antibonding character of the 5a<sub>2</sub> orbital, the calculated first IP of the dimer (6.02 eV) is significantly smaller than that of the monomer (6.62 eV), in agreement with the experimental result that oxidation of Ln(Por)<sub>2</sub> is remarkably easy compared to that of MPor.

Concerning the reduction, the added electron in YbP<sub>2</sub> occupies the P<sub>2</sub>-5a<sub>2</sub> orbital and the calculated EA is very negative (-2.98 eV). This is in contrast to YbP(acac). Addition of an electron to the 4f-like orbital 12b<sub>2</sub> yields a significantly smaller EA. This is again in accord with the experimental fact that Ln<sup>III</sup>(Por)<sub>2</sub> is much easier to reduce than the corresponding monoporphyrin.<sup>16</sup> In the case of Ce<sup>IV</sup>P<sub>2</sub>, the reduction involves addition of an electron to the LUMO (15e<sub>3</sub>/f), giving the anion with Ce<sup>III</sup>.

[CeP<sub>2</sub>]<sup>+</sup> has a ground-state configuration of (5a<sub>2</sub>)<sup>1</sup>. Therefore, neutral YbP<sub>2</sub> is electronically similar to the Ce<sup>IV</sup> sandwich porphyrin cation radical. The structural change from CeP<sub>2</sub> to [CeP<sub>2</sub>]<sup>+</sup> is smaller than that from YbP<sub>2</sub> to [YbP<sub>2</sub>]<sup>+</sup>.

**3.1.3. YbHP<sub>2</sub>.** The ground state of YbHP<sub>2</sub>, (15b<sub>2</sub>/f)<sup>1</sup>(10a<sub>2</sub>)<sup>2</sup>, actually corresponds to that of YbP<sub>2</sub> by addition of one electron to 5a<sub>2</sub>. Thus, the oxidation state of Yb in YbHP<sub>2</sub> is still +3. Magnetic susceptibility measurements of YbH(Por)<sub>2</sub> yield values of magnetic moments typical for the trivalent oxidation state.<sup>29</sup> The experimental result is supported by the calculation. A (15b<sub>2</sub>/f)<sup>2</sup>(10a<sub>2</sub>)<sup>1</sup> state is 0.43 eV higher in energy (see Table 2). With the 10a<sub>2</sub> orbital doubly occupied, YbH(Por)<sub>2</sub> is no longer a  $\pi$ -radical. This was verified through ESR spectroscopy in solution and pure solid.<sup>29</sup> The orbital energy level diagram of YbHP<sub>2</sub> is illustrated in Figure 4. There is a large downshift of the 4f-like orbitals on going from YbP<sub>2</sub> to YbHP<sub>2</sub> so that these orbitals now fall well below the porphyrin 10a<sub>2</sub> and 23a<sub>1</sub> orbitals.

As illustrated in Figure 1d, the molecular structure of YbHP<sub>2</sub> is asymmetric, where one porphyrin is bonded with an axial H atom and other one is not. The complex may be expressed as Yb(HP)(P), where the porphyrin (P) and the protonated porphyrin (HP) represent different subunits. Table 3 shows that the distances from Yb to the N4 planes of HP and P are rather different, with  $R_{\text{Ct}(\text{N}4)\cdots\text{Yb}}$  in HP being larger than that in P. Correspondingly, the core size ( $R_{\text{Ct}(\text{N}4)\cdots\text{N}}$ ) of HP is somewhat smaller than that of P, but the doming of the ring is more significant in HP than in P.

Owing to a small downshift of the valence P<sub>2</sub>-a<sub>2</sub> orbital, the calculated first IP of YbHP<sub>2</sub> is also slightly larger than that of YbP<sub>2</sub>. The reduction of YbHP<sub>2</sub> now involves addition of an electron to the 4f-like orbital 15b<sub>2</sub>, and the calculated EA for this complex is smaller than that for YbP<sub>2</sub>. The negative ion [YbP<sub>2</sub>]<sup>-</sup> has the same ground state as YbHP<sub>2</sub> does, and so it is also not a  $\pi$ -radical. The nonradical character of [Yb(Por)<sub>2</sub>]<sup>-</sup> is supported by the optical properties, since no near-IR band was detected

**3.2. Electron Excitation Energies.** Tables 4–9 report the TDDFT calculated excitation energies ( $E^{\text{exc}}$ ) and oscillator strengths ( $f$ ) for the allowed transitions from the ground state to excited states in YbP(acac), YbP<sub>2</sub>, CeP<sub>2</sub>, [CeP<sub>2</sub>]<sup>+</sup>, YbHP<sub>2</sub>, and [YbP<sub>2</sub>]<sup>-</sup>, respectively. Experimental data<sup>13,21,22,29</sup> for each system are provided for comparison.

**3.2.1. YbP(acac).** For a ‘normal’ planar metal porphyrin (e.g., MgPor, NiPor, or ZnPor), the HOMO and HOMO - 1 are the

**TABLE 4: Calculated Excitation Energies ( $E^{\text{exc}}$ ) and Oscillator Strengths ( $f$ ) for YbP(acac)**

state	contribution (%) <sup>a</sup>	$E^{\text{exc}}$ , eV		$f$	assignment <sup>c</sup>
		calc	exptl <sup>b</sup>		
1 <sup>2</sup> B <sub>1</sub>	99 (30a <sub>1</sub> → 24b <sub>1</sub> )	0.15		0.2 × 10 <sup>-4</sup>	f → f
2 <sup>2</sup> B <sub>1</sub>	90 (29a <sub>1</sub> → 24b <sub>1</sub> )	0.26		0.4 × 10 <sup>-4</sup>	f → f
3 <sup>2</sup> B <sub>1</sub>	91 (28a <sub>1</sub> → 24b <sub>1</sub> )	0.42		0.3 × 10 <sup>-4</sup>	R → M
2 <sup>2</sup> A <sub>1</sub>	79 (22b <sub>1</sub> → 24b <sub>1</sub> ); 20 (21b <sub>1</sub> → 24b <sub>1</sub> )	0.75		0.0035	R → M
4 <sup>2</sup> A <sub>1</sub>	71 (21b <sub>1</sub> → 24b <sub>1</sub> ); 17 (22b <sub>1</sub> → 24b <sub>1</sub> )	1.71		0.0327	R → M
7 <sup>2</sup> B <sub>1</sub>	96 (25a <sub>1</sub> → 24b <sub>1</sub> )	1.86		0.0041	R → M
9 <sup>2</sup> B <sub>1</sub>	99 (14a <sub>2</sub> → 21b <sub>2</sub> )	2.06	2.08 (0.7)	0.4 × 10 <sup>-7</sup>	Q'
4 <sup>2</sup> B <sub>2</sub>	99 (14a <sub>2</sub> → 25b <sub>1</sub> )	2.06		0.3 × 10 <sup>-8</sup>	
5 <sup>2</sup> A <sub>1</sub>	93 (19b <sub>1</sub> → 24b <sub>1</sub> )	2.08		0.0049	R → M
8 <sup>2</sup> B <sub>2</sub>	98 (28a <sub>1</sub> → 21b <sub>2</sub> )	2.58	2.23 (2.4)	0.0011	Q
13 <sup>2</sup> B <sub>1</sub>	98 (28a <sub>1</sub> → 25b <sub>1</sub> )	2.58		0.0009	
10 <sup>2</sup> A <sub>1</sub>	50 (24b <sub>1</sub> → 25b <sub>1</sub> ); 39 (20b <sub>2</sub> → 21b <sub>2</sub> )	2.74		0.0014	M → R
15 <sup>2</sup> B <sub>1</sub>	95 (23a <sub>1</sub> → 24b <sub>1</sub> )	2.83		0.0124	R → M
12 <sup>2</sup> B <sub>2</sub>	99 (23b <sub>1</sub> → 15a <sub>2</sub> )	3.06		0.0015	
18 <sup>2</sup> B <sub>1</sub>	66 (19b <sub>2</sub> → 15a <sub>2</sub> ); 17 (20b <sub>2</sub> → 15a <sub>2</sub> )	3.13		0.0018	M → R
13 <sup>2</sup> B <sub>2</sub>	43 (28a <sub>1</sub> → 21b <sub>2</sub> ); 35 (27a <sub>1</sub> → 21b <sub>2</sub> )	3.15	2.90 (48)	0.1363	B
19 <sup>2</sup> B <sub>1</sub>	52 (28a <sub>1</sub> → 25b <sub>1</sub> ); 41 (27a <sub>1</sub> → 25b <sub>1</sub> )	3.17		0.0408	
19 <sup>2</sup> A <sub>1</sub>	82 (17b <sub>2</sub> → 21b <sub>2</sub> )	3.21		0.0014	
21 <sup>2</sup> B <sub>1</sub>	67 (27a <sub>1</sub> → 25b <sub>1</sub> )	3.25	3.03 (5.0)	0.1202	B'
14 <sup>2</sup> B <sub>2</sub>	60 (27a <sub>1</sub> → 21b <sub>2</sub> )	3.25		0.1635	
20 <sup>2</sup> A <sub>1</sub>	87 (13a <sub>2</sub> → 15a <sub>2</sub> )	3.26		0.0049	M → R
23 <sup>2</sup> B <sub>1</sub>	53 (26a <sub>1</sub> → 25b <sub>1</sub> )	3.29		0.2335	
16 <sup>2</sup> B <sub>2</sub>	50 (26a <sub>1</sub> → 21b <sub>2</sub> ); 11 (27a <sub>1</sub> → 21b <sub>2</sub> )	3.30		0.2058	
17 <sup>2</sup> B <sub>2</sub>	74 (11a <sub>2</sub> → 24b <sub>1</sub> ); 20 (24b <sub>1</sub> → 15a <sub>2</sub> )	3.33		0.0047	R → M
18 <sup>2</sup> B <sub>2</sub>	62 (24b <sub>1</sub> → 15a <sub>2</sub> ); 21 (11a <sub>2</sub> → 24b <sub>1</sub> )	3.35		0.0101	M → R
24 <sup>2</sup> B <sub>1</sub>	49 (26a <sub>1</sub> → 25b <sub>1</sub> ); 25 (27a <sub>1</sub> → 25b <sub>1</sub> )	3.36		0.1775	EB <sub>1</sub>
19 <sup>2</sup> B <sub>2</sub>	45 (26a <sub>1</sub> → 21b <sub>2</sub> ); 17 (27a <sub>1</sub> → 21b <sub>2</sub> ); 15 (24b <sub>1</sub> → 15a <sub>2</sub> )	3.37		0.1329	
25 <sup>2</sup> B <sub>1</sub>	67 (19b <sub>2</sub> → 15a <sub>2</sub> ); 19 (20b <sub>2</sub> → 15a <sub>2</sub> )	3.49		0.0019	
26 <sup>2</sup> B <sub>1</sub>	55 (18b <sub>2</sub> → 15a <sub>2</sub> ); 18 (19b <sub>2</sub> → 15a <sub>2</sub> )	3.57		0.0258	
21 <sup>2</sup> B <sub>2</sub>	59 (26a <sub>1</sub> → 21b <sub>2</sub> ); 22 (23b <sub>1</sub> → 16a <sub>2</sub> )	3.60		0.2301	EB <sub>2</sub>

<sup>a</sup> A contribution of less than 10% is not listed; the same is true for other tables. <sup>b</sup> Experimental data for YbTPP(acac), ref 13; the values in parentheses are the absorbance intensity ( $\epsilon 10^{-4}$ ) in  $\text{dm}^3\text{mol}^{-1}\text{cm}^{-1}$ . <sup>c</sup> M = metal and R = ring.

**TABLE 5: Calculated Excitation Energies ( $E^{\text{exc}}$ ) and Oscillator Strengths ( $f$ ) for YbP<sub>2</sub>**

state	contribution (%)	$E^{\text{exc}}$ , eV		$f$	assignment
		calc	exptl <sup>a</sup>		
1 <sup>3</sup> B <sub>2</sub>	100 (11a <sub>1</sub> → 12b <sub>2</sub> )	0.11		0.0004	R → M
2 <sup>3</sup> B <sub>2</sub>	93 (5b <sub>1</sub> → 5a <sub>2</sub> )	1.15	1.08 (3.83)	0.0713	near-IR
3 <sup>3</sup> E <sub>1</sub>	98 (14e <sub>3</sub> → 12b <sub>2</sub> )	1.25		0.0016	R → M
3 <sup>3</sup> B <sub>2</sub>	95 (15e <sub>3</sub> → 17e <sub>1</sub> ) ( $\beta$ )	1.34		0.0117	M → R
6 <sup>3</sup> E <sub>1</sub>	96 (15e <sub>1</sub> → 5a <sub>2</sub> )	1.50		0.0026	
4 <sup>3</sup> B <sub>2</sub>	97 (15e <sub>3</sub> → 17e <sub>1</sub> ) ( $\alpha$ )	1.60		0.0043	M → R
5 <sup>3</sup> B <sub>2</sub>	97 (16e <sub>1</sub> → 16e <sub>3</sub> )	1.63		0.0012	M → R
8 <sup>3</sup> E <sub>1</sub>	75 (12b <sub>2</sub> → 16e <sub>3</sub> ); 16 (11b <sub>2</sub> → 16e <sub>3</sub> )	1.73		0.0014	M → R
6 <sup>3</sup> B <sub>2</sub>	99 (10a <sub>1</sub> → 12b <sub>2</sub> )	1.90		0.0171	R → M
11 <sup>3</sup> E <sub>1</sub>	62 (5a <sub>2</sub> → 17e <sub>1</sub> ); 29 (14e <sub>1</sub> → 5a <sub>2</sub> )	2.01	1.85 (3.21)	0.0030	Q <sub>1</sub>
13 <sup>3</sup> E <sub>1</sub>	56 (14e <sub>1</sub> → 5a <sub>2</sub> ); 19 (11a <sub>2</sub> → 17e <sub>1</sub> ); 16 (5a <sub>2</sub> → 17e <sub>1</sub> )	2.12		0.0040	
16 <sup>3</sup> E <sub>1</sub>	68 (5b <sub>1</sub> → 16e <sub>3</sub> ); 12 (11a <sub>1</sub> → 17e <sub>1</sub> )	2.34	2.34 (3.76)	0.0052	Q <sub>2</sub>
18 <sup>3</sup> E <sub>1</sub>	95 (13e <sub>3</sub> → 12b <sub>2</sub> )	2.51		0.0012	R → M
19 <sup>3</sup> E <sub>1</sub>	95 (11b <sub>2</sub> → 16e <sub>3</sub> )	2.55	2.49 (3.75)	0.0018	Q <sub>3</sub>
21 <sup>3</sup> E <sub>1</sub>	92 (12e <sub>3</sub> → 12b <sub>2</sub> )	2.65		0.0098	R → M
23 <sup>3</sup> E <sub>1</sub>	97 (14e <sub>2</sub> → 16e <sub>3</sub> )	2.81		0.0032	
11 <sup>3</sup> B <sub>2</sub>	89 (15e <sub>1</sub> → 16e <sub>3</sub> )	3.08		0.0104	
26 <sup>3</sup> E <sub>1</sub>	81 (10b <sub>2</sub> → 16e <sub>3</sub> )	3.13		0.0948	
28 <sup>3</sup> E <sub>1</sub>	96 (14e <sub>2</sub> → 17e <sub>1</sub> )	3.29		0.0096	
13 <sup>3</sup> B <sub>2</sub>	89 (14e <sub>3</sub> → 17e <sub>1</sub> )	3.41		0.0175	
29 <sup>3</sup> E <sub>1</sub>	90 (13e <sub>2</sub> → 16e <sub>3</sub> )	3.61		0.0978	
30 <sup>3</sup> E <sub>1</sub>	38 (13e <sub>2</sub> → 16e <sub>3</sub> ); 33 (16e <sub>1</sub> → 16e <sub>2</sub> )	3.65	3.35 (4.98)	0.3866	B
31 <sup>3</sup> E <sub>1</sub>	60 (16e <sub>1</sub> → 16e <sub>2</sub> ); 31 (13e <sub>2</sub> → 16e <sub>3</sub> )	3.67		0.0662	
32 <sup>3</sup> E <sub>1</sub>	33 (13e <sub>2</sub> → 16e <sub>3</sub> ); 10 (5b <sub>1</sub> → 16e <sub>3</sub> )	3.74		0.7508	
16 <sup>3</sup> B <sub>2</sub>	96 (9a <sub>1</sub> → 12b <sub>2</sub> )	3.75		0.0050	R → M
33 <sup>3</sup> E <sub>1</sub>	95 (10a <sub>1</sub> → 17e <sub>1</sub> )	3.84		0.0192	

<sup>a</sup> Experimental data for YbOEP<sub>2</sub>, ref 22; the values in parentheses are the absorbance intensity ( $\log \epsilon$ ) in  $\text{dm}^3\text{mol}^{-1}\text{cm}^{-1}$ .

porphyrin a<sub>2u</sub> and a<sub>1u</sub>, respectively, which are nearly degenerate and well separated from lower-lying levels. The excitations from the (a<sub>2u</sub>, a<sub>1u</sub>) to the LUMO (e<sub>g</sub>), which lead to the two lowest excited states 1<sup>1</sup>E<sub>u</sub> and 2<sup>1</sup>E<sub>u</sub>, give rise to a weak absorption band Q in the visible and a very strong B (or Soret) band in the

near-ultraviolet (UV).<sup>47</sup> (For the a<sub>1u</sub>, a<sub>2u</sub>, and e<sub>g</sub> orbitals mentioned here, refer to the orbital energy level diagram of YbP-D<sub>4h</sub> in Figure 2).

Experimental spectral data are available for YbTPP(acac)<sup>13</sup> and are shown to be different from those of a normal MPor.

**TABLE 6: Calculated Excitation Energies ( $E^{\text{exc}}$ ) and Oscillator Strengths ( $f$ ) for CeP<sub>2</sub>**

state	contribution (%)	$E^{\text{exc}}$ , eV		$f$	assignment
		calc	exptl <sup>a</sup>		
1 <sup>1</sup> B <sub>2</sub>	100 (11a <sub>1</sub> → 12b <sub>2</sub> )	0.87		0.0043	R → M
2 <sup>1</sup> B <sub>2</sub>	93 (15e <sub>1</sub> → 15e <sub>3</sub> )	1.69		0.0038	R → M
3 <sup>1</sup> B <sub>2</sub>	77 (14e <sub>2</sub> → 15e <sub>2</sub> ); 20 (14e <sub>3</sub> → 16e <sub>1</sub> )	1.76		0.0011	R → M
7 <sup>1</sup> E <sub>1</sub>	92 (10b <sub>2</sub> → 15e <sub>3</sub> )	1.78		0.0020	R → M
4 <sup>1</sup> B <sub>2</sub>	79 (14e <sub>3</sub> → 16e <sub>1</sub> ); 16 (14e <sub>2</sub> → 15e <sub>2</sub> )	1.87	1.94	0.0317	Q'
12 <sup>1</sup> E <sub>1</sub>	68 (5a <sub>2</sub> → 17e <sub>1</sub> )	2.12	2.16	0.0102	Q
6 <sup>1</sup> B <sub>2</sub>	99 (13e <sub>1</sub> → 15e <sub>3</sub> )	2.40		0.0069	R → M
7 <sup>1</sup> B <sub>2</sub>	99 (10a <sub>1</sub> → 12b <sub>2</sub> )	2.56		0.0111	R → M
16 <sup>1</sup> E <sub>1</sub>	93 (13e <sub>1</sub> → 15e <sub>2</sub> )	2.67	2.66	0.0096	Q''
18 <sup>1</sup> E <sub>1</sub>	98 (9b <sub>2</sub> → 15e <sub>3</sub> )	2.81		0.0028	R → M
19 <sup>1</sup> E <sub>1</sub>	95 (14e <sub>2</sub> → 16e <sub>3</sub> )	2.84		0.0090	
20 <sup>1</sup> E <sub>1</sub>	84 (13e <sub>2</sub> → 16e <sub>1</sub> )	3.01		0.0526	R → M
8 <sup>1</sup> B <sub>2</sub>	49 (13e <sub>2</sub> → 15e <sub>2</sub> ); (13e <sub>2</sub> → 16e <sub>1</sub> )	3.05		0.0036	R → M
21 <sup>1</sup> E <sub>1</sub>	97 (13e <sub>3</sub> → 15e <sub>2</sub> )	3.06		0.0024	R → M
9 <sup>1</sup> B <sub>2</sub>	53 (13e <sub>3</sub> → 16e <sub>1</sub> ); 24 (15e <sub>1</sub> → 16e <sub>3</sub> ); 20 (13e <sub>2</sub> → 15e <sub>2</sub> )	3.07		0.0026	R → M
22 <sup>1</sup> E <sub>1</sub>	55 (10b <sub>2</sub> → 16e <sub>3</sub> ); 15 (13e <sub>3</sub> → 12b <sub>2</sub> ); 11 (13e <sub>2</sub> → 16e <sub>1</sub> )	3.12		0.1190	
10 <sup>1</sup> B <sub>2</sub>	50 (15e <sub>1</sub> → 16e <sub>3</sub> ); 29 (13e <sub>2</sub> → 15e <sub>2</sub> ); 13 (14e <sub>3</sub> → 17e <sub>1</sub> )	3.12		0.0223	
23 <sup>1</sup> E <sub>1</sub>	79 (13e <sub>3</sub> → 12b <sub>2</sub> ); 20 (10b <sub>2</sub> → 16e <sub>3</sub> )	3.17		0.0048	R → M
24 <sup>1</sup> E <sub>1</sub>	94 (14e <sub>2</sub> → 17e <sub>1</sub> )	3.26		0.0224	
11 <sup>1</sup> B <sub>2</sub>	82 (14e <sub>3</sub> → 17e <sub>1</sub> ); 14 (15e <sub>1</sub> → 16e <sub>3</sub> )	3.38		0.0079	
25 <sup>1</sup> E <sub>1</sub>	98 (12e <sub>2</sub> → 15e <sub>3</sub> )	3.39		0.0166	R → M
26 <sup>1</sup> E <sub>1</sub>	33 (12e <sub>3</sub> → 15e <sub>2</sub> ); 10 (12e <sub>3</sub> → 12b <sub>2</sub> ); 10 (10b <sub>2</sub> → 16e <sub>3</sub> ); 10 (5b <sub>1</sub> → 16e <sub>3</sub> )	3.54	3.28	0.9188	B
27 <sup>1</sup> E <sub>1</sub>	54 (12e <sub>3</sub> → 15e <sub>2</sub> ); 35 (12e <sub>3</sub> → 12b <sub>2</sub> )	3.64		0.1836	R → M
12 <sup>1</sup> B <sub>2</sub>	91 (13e <sub>1</sub> → 16e <sub>3</sub> )	3.66		0.0101	
29 <sup>1</sup> E <sub>1</sub>	48 (12e <sub>3</sub> → 12b <sub>2</sub> ); 11 (12e <sub>3</sub> → 15e <sub>2</sub> )	3.80		0.8446	R → M
30 <sup>1</sup> E <sub>1</sub>	92 (10a <sub>1</sub> → 17e <sub>1</sub> )	3.93		0.1212	

<sup>a</sup> Experimental data for Ce(OEP)<sub>2</sub>, ref 21.**TABLE 7: Calculated Excitation Energies ( $E^{\text{exc}}$ ) and Oscillator Strengths ( $f$ ) for [CeP<sub>2</sub>]<sup>+</sup>**

state	contribution (%)	$E^{\text{exc}}$ , eV		$f$	assignment
		calc	exptl <sup>a</sup>		
2 <sup>2</sup> B <sub>2</sub>	89 (11a <sub>1</sub> → 12b <sub>2</sub> ); 11 (5b <sub>1</sub> → 5a <sub>2</sub> )	0.81		0.0007	R → M
3 <sup>2</sup> B <sub>2</sub>	85 (5b <sub>1</sub> → 5a <sub>2</sub> )	1.02	0.98	0.0573	near-IR
10 <sup>2</sup> E <sub>1</sub>	53 (15e <sub>1</sub> → 5a <sub>2</sub> ); 42 (14e <sub>1</sub> → 15e <sub>3</sub> )	1.43		0.0022	
5 <sup>2</sup> B <sub>2</sub>	81 (15e <sub>1</sub> → 15e <sub>3</sub> ); 15 (14e <sub>2</sub> → 15e <sub>2</sub> )	1.68		0.0028	R → M
14 <sup>2</sup> E <sub>1</sub>	46 (10b <sub>2</sub> → 15e <sub>3</sub> ); 26 (14e <sub>2</sub> → 16e <sub>1</sub> )	1.73		0.0032	R → M
9 <sup>2</sup> B <sub>2</sub>	70 (14e <sub>3</sub> → 16e <sub>1</sub> ); 10 (14e <sub>2</sub> → 15e <sub>2</sub> )	1.84		0.0453	R → M
21 <sup>2</sup> E <sub>1</sub>	83 (14e <sub>1</sub> → 5a <sub>2</sub> )	1.95		0.0022	
25 <sup>2</sup> E <sub>1</sub>	55 (5a <sub>2</sub> → 17e <sub>1</sub> ); 14 (5b <sub>1</sub> → 16e <sub>3</sub> ); 13 (11a <sub>2</sub> → 17e <sub>1</sub> ); 11 (13e <sub>1</sub> → 5a <sub>2</sub> )	2.14		0.0042	
29 <sup>2</sup> E <sub>1</sub>	39 (5b <sub>1</sub> → 16e <sub>3</sub> ); 33 (10a <sub>1</sub> → 16e <sub>1</sub> )	2.38	2.41	0.0030	Q
30 <sup>2</sup> E <sub>1</sub>	60 (10a <sub>1</sub> → 16e <sub>1</sub> ); 31 (5b <sub>1</sub> → 16e <sub>3</sub> )	2.39		0.0044	R → M
13 <sup>2</sup> B <sub>2</sub>	99 (13e <sub>1</sub> → 15e <sub>3</sub> )	2.43		0.0062	R → M
15 <sup>2</sup> B <sub>2</sub>	97 (10a <sub>1</sub> → 12b <sub>2</sub> )	2.52		0.0137	R → M
34 <sup>2</sup> E <sub>1</sub>	56 (13e <sub>1</sub> → 15e <sub>2</sub> ); 31 (14e <sub>2</sub> → 16e <sub>3</sub> )	2.69		0.0040	R → M
35 <sup>2</sup> E <sub>1</sub>	57 (14e <sub>2</sub> → 16e <sub>3</sub> ); 39 (13e <sub>1</sub> → 15e <sub>2</sub> )	2.70		0.0068	R → M
38 <sup>2</sup> E <sub>1</sub>	94 (14e <sub>2</sub> → 16e <sub>3</sub> )	2.80		0.0072	
40 <sup>2</sup> E <sub>1</sub>	98 (9b <sub>2</sub> → 15e <sub>3</sub> )	2.84		0.0048	R → M
41 <sup>2</sup> E <sub>1</sub>	96 (10b <sub>2</sub> → 16e <sub>3</sub> )	2.98		0.0036	
42 <sup>2</sup> E <sub>1</sub>	51 (13e <sub>2</sub> → 16e <sub>3</sub> ); 26 (10b <sub>2</sub> → 16e <sub>3</sub> )	3.01		0.0682	
43 <sup>2</sup> E <sub>1</sub>	97 (13e <sub>2</sub> → 16e <sub>1</sub> )	3.02		0.0032	R → M
45 <sup>2</sup> E <sub>1</sub>	47 (10b <sub>2</sub> → 16e <sub>3</sub> ); 45 (13e <sub>2</sub> → 16e <sub>1</sub> )	3.08		0.0116	
48 <sup>2</sup> E <sub>1</sub>	96 (13e <sub>2</sub> → 12b <sub>2</sub> ) ( $\beta$ )	3.16		0.0162	R → M
49 <sup>2</sup> E <sub>1</sub>	95 (13e <sub>3</sub> → 12b <sub>2</sub> ) ( $\alpha$ )	3.23		0.0282	R → M
50 <sup>2</sup> E <sub>1</sub>	94 (14e <sub>2</sub> → 17e <sub>1</sub> )	3.25		0.0308	
52 <sup>2</sup> E <sub>1</sub>	99 (12e <sub>2</sub> → 15e <sub>3</sub> )	3.44		0.0132	R → M
53 <sup>2</sup> E <sub>1</sub>	31 (12e <sub>3</sub> → 15e <sub>2</sub> ); 12 (5b <sub>1</sub> → 16e <sub>3</sub> ); 10 (12e <sub>3</sub> → 12b <sub>2</sub> )	3.57	3.44	0.9930	B
54 <sup>2</sup> E <sub>1</sub>	98 (12e <sub>3</sub> → 15e <sub>2</sub> )	3.59		0.0166	R → M
56 <sup>2</sup> E <sub>1</sub>	51 (12e <sub>3</sub> → 15e <sub>2</sub> ); 33 (12e <sub>3</sub> → 12b <sub>2</sub> )	3.67		0.1830	R → M
60 <sup>2</sup> E <sub>1</sub>	49 (12e <sub>3</sub> → 12b <sub>2</sub> )	3.84		0.7058	R → M

<sup>a</sup> Experimental data for [Ce(OEP)<sub>2</sub>]<sup>+</sup>, refs 20 and 21.

They exhibit two weak absorption bands (assigned as Q' and Q) and two strong absorption bands (assigned as B and B'). The multiple bands in the Q and B regions are supported by the calculations on YbP(acac). Because there is no split between the 25b<sub>1</sub> and 21b<sub>2</sub> orbitals, the excitation energies for the transitions from an orbital to 25b<sub>1</sub> and 21b<sub>2</sub> are the same or nearly the same. The Q' and Q bands are assigned to the 9<sup>2</sup>B<sub>1</sub>/4<sup>2</sup>B<sub>2</sub> and 8<sup>2</sup>B<sub>2</sub>/13<sup>2</sup>B<sub>1</sub> states, respectively, which are nearly pure

14a<sub>2</sub> → 21b<sub>2</sub>/25b<sub>1</sub> and 28a<sub>1</sub> → 21b<sub>2</sub>/25b<sub>1</sub> transitions. Here, 14a<sub>2</sub> and 28a<sub>1</sub> are the porphyrin a<sub>1u</sub> and a<sub>2u</sub> orbitals, respectively. For a normal MPor, a<sub>1u</sub> and a<sub>2u</sub> are nearly degenerate and the Q and B bands just arise from a mixture of the a<sub>1u</sub> → e<sub>g</sub> and a<sub>2u</sub> → e<sub>g</sub> transitions; that is, Q is described by a plus combination of the a<sub>1u</sub> → e<sub>g</sub> and a<sub>2u</sub> → e<sub>g</sub> transitions while B is described by a minus combination of the a<sub>1u</sub> → e<sub>g</sub> and a<sub>2u</sub> → e<sub>g</sub> transitions. In the case of YbP(acac), the 14a<sub>2</sub> and 28a<sub>1</sub> orbitals are separated

**TABLE 8: Calculated Excitation Energies ( $E^{\text{exc}}$ ) and Oscillator Strengths ( $f$ ) for YbHP<sub>2</sub>**

state	contribution (%)	$E^{\text{exc}}$ , eV		$f$	assignment
		calc	exptl <sup>a</sup>		
3 <sup>2</sup> E	88 (29e → 15b <sub>2</sub> )	0.49		0.0036	R → M
1 <sup>2</sup> A <sub>1</sub>	91 (14b <sub>2</sub> → 15b <sub>2</sub> )	0.77		0.0030	R → M
5 <sup>2</sup> E	100 (27e → 15b <sub>2</sub> )	1.23		0.0014	R → M
3 <sup>2</sup> A <sub>1</sub>	97 (23a <sub>1</sub> → 24a <sub>1</sub> )	1.51		0.0253	R → H <sub>(ax)</sub>
5 <sup>2</sup> A <sub>1</sub>	70 (13b <sub>2</sub> → 15b <sub>2</sub> ); 19 (22a <sub>1</sub> → 24a <sub>1</sub> )	1.84		0.0140	R → M
15 <sup>2</sup> E	69 (10a <sub>2</sub> → 33e)	2.12	2.04 (3.50)	0.0068	Q <sub>1</sub>
19 <sup>2</sup> E	73 (22a <sub>1</sub> → 32e)	2.25	2.23 (3.87)	0.0003	Q <sub>2</sub>
27 <sup>2</sup> E	69 (22a <sub>1</sub> → 33e)	2.59	2.53 (3.92)	0.0034	Q <sub>3</sub>
28 <sup>2</sup> E	47 (21a <sub>1</sub> → 32e); 22 (15b <sub>2</sub> → 32e)	2.64		0.0086	M → R
33 <sup>2</sup> E	24 (28e → 24a <sub>1</sub> ); 23 (21a <sub>1</sub> → 32e); 15 (29e → 24a <sub>1</sub> )	2.78		0.0296	R → H <sub>(ax)</sub>
15 <sup>2</sup> A <sub>1</sub>	82 (29e → 32e); 10 (31e → 32e)	2.83		0.0050	
37 <sup>2</sup> E	93 (28e → 24a <sub>1</sub> )	2.98		0.0030	R → H <sub>(ax)</sub>
38 <sup>2</sup> E	35 (14b <sub>1</sub> → 32e); 33 (15b <sub>1</sub> → 32e)	3.00		0.0054	
41 <sup>2</sup> E	44 (21a <sub>1</sub> → 33e); 25 (20a <sub>1</sub> → 32e); 12 (9a <sub>2</sub> → 33e)	3.06		0.0058	M → R
42 <sup>2</sup> E	82 (14b <sub>1</sub> → 32e)	3.08		0.0060	
44 <sup>2</sup> E	40 (21a <sub>1</sub> → 33e); 25 (9a <sub>2</sub> → 33e)	3.17	3.06 (5.42)	0.0376	B
45 <sup>2</sup> E	54 (14b <sub>2</sub> → 33e); 39 (15b <sub>2</sub> → 33e)	3.21		0.0016	
47 <sup>2</sup> E	75 (27e → 24a <sub>1</sub> ); 19 (21a <sub>1</sub> → 33e)	3.28		0.0128	R → H <sub>(ax)</sub>
49 <sup>2</sup> E	51 (21a <sub>1</sub> → 33e); 11 (20a <sub>1</sub> → 33e)	3.34		0.0050	
51 <sup>2</sup> E	68 (14b <sub>1</sub> → 33e); 23 (15b <sub>1</sub> → 33e)	3.40		0.0026	
54 <sup>2</sup> E	96 (23e → 15b <sub>2</sub> )	3.54		0.0012	R → M
55 <sup>2</sup> E	41 (20a <sub>1</sub> → 33e)	3.60		0.2274	EB <sub>1</sub>
56 <sup>2</sup> E	91 (19a <sub>1</sub> → 32e)	3.63		0.0130	
57 <sup>2</sup> E	100 (22e → 15b <sub>2</sub> )	3.71		0.0018	R → M
58 <sup>2</sup> E	40 (20a <sub>1</sub> → 33e)	3.73		0.6314	EB <sub>2</sub>

<sup>a</sup> Experimental data for YbH(TPP)<sub>2</sub>, ref 29; the values in parentheses are the absorbance intensity (log  $\epsilon$ ) in dm<sup>3</sup>mol<sup>-1</sup>cm<sup>-1</sup>.

**TABLE 9: Calculated Excitation Energies ( $E^{\text{exc}}$ ) and Oscillator Strengths ( $f$ ) for [YbP<sub>2</sub>]<sup>-</sup>**

state	contribution (%)	$E^{\text{exc}}$ , eV		$f$	assignment
		calc	exptl <sup>a</sup>		
1 <sup>2</sup> B <sub>2</sub>	100 (11a <sub>1</sub> → 12b <sub>2</sub> )	0.17		0.0024	R → M
2 <sup>2</sup> B <sub>2</sub>	100 (15e <sub>3</sub> → 17e <sub>1</sub> )	1.21		0.0026	M → R
3 <sup>2</sup> E <sub>1</sub>	98 (14e <sub>3</sub> → 12b <sub>2</sub> )	1.28		0.0016	
3 <sup>2</sup> B <sub>2</sub>	99 (15e <sub>3</sub> → 17e <sub>1</sub> )	1.54		0.0016	M → R
5 <sup>2</sup> B <sub>2</sub>	100 (10a <sub>1</sub> → 12b <sub>2</sub> )	1.93		0.0092	R → M
11 <sup>2</sup> E <sub>1</sub>	71 (5a <sub>2</sub> → 17e <sub>1</sub> ); 12 (11a <sub>1</sub> → 17e <sub>1</sub> )	2.07	1.94 (3.46)	0.0082	Q <sub>1</sub>
13 <sup>2</sup> E <sub>1</sub>	70 (5b <sub>1</sub> → 16e <sub>3</sub> ); 18 (11a <sub>1</sub> → 17e <sub>1</sub> )	2.24	2.03 (3.48)	0.0007	Q <sub>2</sub>
14 <sup>2</sup> E <sub>1</sub>	66 (5b <sub>1</sub> → 16e <sub>3</sub> ); 24 (11a <sub>1</sub> → 17e <sub>1</sub> )	2.28	2.21 (3.90)	0.0042	Q <sub>3</sub>
17 <sup>2</sup> E <sub>1</sub>	96 (11b <sub>2</sub> → 16e <sub>3</sub> )	2.54	2.37 (3.80)	0.0020	Q <sub>4</sub>
18 <sup>2</sup> E <sub>1</sub>	91 (12e <sub>3</sub> → 12b <sub>2</sub> )	2.63	2.53 (4.12)	0.0158	Q <sub>5</sub>
20 <sup>2</sup> E <sub>1</sub>	96 (14e <sub>2</sub> → 16e <sub>3</sub> )	2.77	2.62 (4.15)	0.0028	Q <sub>6</sub>
10 <sup>2</sup> B <sub>2</sub>	88 (15e <sub>1</sub> → 16e <sub>3</sub> ); 11 (14e <sub>3</sub> → 17e <sub>1</sub> )	3.03		0.0070	
23 <sup>2</sup> E <sub>1</sub>	82 (10b <sub>2</sub> → 16e <sub>3</sub> ); 17 (14e <sub>2</sub> → 17e <sub>1</sub> )	3.11		0.0014	
24 <sup>2</sup> E <sub>1</sub>	75 (10b <sub>2</sub> → 16e <sub>3</sub> )	3.14	3.05 (5.67)	0.1516	B
25 <sup>2</sup> E <sub>1</sub>	94 (14e <sub>2</sub> → 17e <sub>1</sub> )	3.19		0.0026	
12 <sup>2</sup> B <sub>2</sub>	87 (14e <sub>3</sub> → 17e <sub>1</sub> ); 10 (15e <sub>1</sub> → 16e <sub>3</sub> )	3.34		0.0128	
26 <sup>2</sup> E <sub>1</sub>	80 (13e <sub>2</sub> → 16e <sub>3</sub> ); 16 (16e <sub>1</sub> → 16e <sub>2</sub> )	3.54		0.0248	
27 <sup>2</sup> E <sub>1</sub>	74 (16e <sub>1</sub> → 16e <sub>2</sub> ); 21 (13e <sub>2</sub> → 16e <sub>3</sub> )	3.55		0.0600	M → R
28 <sup>2</sup> E <sub>1</sub>	70 (13e <sub>2</sub> → 16e <sub>3</sub> )	3.58		0.3006	EB <sub>1</sub>
29 <sup>2</sup> E <sub>1</sub>	26 (13e <sub>2</sub> → 16e <sub>3</sub> ); 12 (5b <sub>1</sub> → 16e <sub>3</sub> ); 10 (10b <sub>2</sub> → 16e <sub>3</sub> )	3.67		0.9008	EB <sub>2</sub>

<sup>a</sup> Experimental data for [Yb(TPP)<sub>2</sub>]<sup>-</sup>, ref 29; the values in parentheses are the absorbance intensity (log  $\epsilon$ ) in dm<sup>3</sup>mol<sup>-1</sup>cm<sup>-1</sup>.

relatively widely and the 14a<sub>2</sub> → 21b<sub>2</sub>/25b<sub>1</sub> and 28a<sub>1</sub> → 21b<sub>2</sub>/25b<sub>1</sub> transitions do not mix, which give rise to just two weak Q bands. Our calculated oscillator strength ( $f$ ) for the Q' band is nearly zero, and it may be underestimated by the TDDFT method. We find that there is a ring to metal (R → M) transition, i.e., 19b<sub>1</sub> → 24b<sub>1</sub>, occurring at 2.08 eV with  $f = 0.005$ . It is possible that the Q' band results from this transition. Since the 4f-shell is open, there exist several R → M transitions with nonnegligible  $f$  to the red of the Q bands. They occur at 0.75, 1.71, and 1.86 eV, respectively, and should contribute to the near-IR region of YbPor(acac). There are also 4f → 4f transitions, which have low excitation energies and very small oscillator strengths.

On the basis of the calculated  $E^{\text{exc}}$  and  $f$ , the two strong B and B' bands are assigned to the 13<sup>2</sup>B<sub>2</sub>/19<sup>2</sup>B<sub>1</sub> and 21<sup>2</sup>B<sub>1</sub>/14<sup>2</sup>B<sub>2</sub>

states, respectively; the former arises from a mixture of the 28a<sub>1</sub> → 21b<sub>2</sub>/25b<sub>1</sub> and 27a<sub>1</sub> → 21b<sub>2</sub>/25b<sub>1</sub> transitions while the latter is mainly from the 27a<sub>1</sub> → 21b<sub>2</sub>/25b<sub>1</sub> transition. According to the calculations, several transitions with large  $f$  are present to the blue of the B bands, but there has been no experimental elucidation of any details about this energy region. Between the Q and B bands, there are some M → R and R → M transitions, which may only contribute to the broadening of the Q or B band. The calculated excitation energies for YbP(acac) are generally 0.2–0.3 eV larger than the spectral data for YbTPP(acac). (For the Q' band, the calculated and experimental results are almost equal.)

3.2.2. *YbP<sub>2</sub>*. Experimental spectral data are available for Yb-(OEP)<sub>2</sub> and show three weak bands, assigned as Q<sub>1</sub>, Q<sub>2</sub>, and Q<sub>3</sub>, and one strong band, assigned as B.<sup>22</sup> In addition, there is



an intermediately strong band at a low energy of 1.08 eV. The presence of an intense near-IR absorption is a remarkable feature of the single-hole Ln<sup>III</sup>(Por)<sub>2</sub> and [Ce<sup>IV</sup>(Por)<sub>2</sub>]<sup>+</sup> species and is attributed to a transition between the two delocalized MOs, namely, 5b<sub>1</sub> → 5a<sub>2</sub>. This is a consequence of the orbital splitting due to ring–ring interaction. Our calculated  $E^{\text{exc}}$  (1.15 eV) and  $f$  (0.0713) for the 5b<sub>1</sub> → 5a<sub>2</sub> transition nicely account for this near-IR absorption.

The Q<sub>1</sub> band is assigned to the 11<sup>3</sup>E<sub>1</sub> state, which is dominated by the 5a<sub>2</sub> → 17e<sub>1</sub> transition (~60%) and includes some participation of the 14e<sub>1</sub> → 5a<sub>2</sub> transition (~30%). Since 5a<sub>2</sub> is an antibonding orbital and lies relatively high, the Q<sub>1</sub> band here is red-shifted with respect to the Q' band of YbP(acac). The Q<sub>2</sub> and Q<sub>3</sub> bands are accounted for by the 5b<sub>1</sub> → 16e<sub>3</sub> and 11b<sub>2</sub> → 16e<sub>3</sub> transitions, respectively. The 30<sup>3</sup>E<sub>1</sub> state ( $E^{\text{exc}} = 3.65$  eV,  $f = 0.3866$ ) is then responsible for the B band, which shows a large mixture of the 13e<sub>2</sub> → 16e<sub>3</sub> and 16e<sub>1</sub> → 16e<sub>2</sub> transitions. There are several R → M and M → R transitions occurring to the red of the Q bands.

The general appearance of the spectrum of Ce(OEP)<sub>2</sub> is similar to that of Yb(OEP)<sub>2</sub> (three weak Q bands and one strong B band), including the absorption maximum positions.<sup>21</sup> This is consistent with the calculations on YbP<sub>2</sub> and CeP<sub>2</sub>. With a doubly occupied 5a<sub>2</sub> orbital, the CeP<sub>2</sub> species does no longer have a characteristic near-IR absorption, different from YbP<sub>2</sub>.

In contrast to neutral Ce(OEP)<sub>2</sub>, the absorption spectrum of [Ce(OEP)<sub>2</sub>]<sup>+</sup> is relatively simple; it exhibits one Q band and one B band.<sup>21</sup> In the cation  $\pi$ -radical, the 5b<sub>1</sub> → 5a<sub>2</sub> transition results in a strong near-IR absorption feature, similar to the situation for Yb(Por)<sub>2</sub>. The calculated  $E^{\text{exc}}$  for this transition (1.02 eV) is close to that observed for [Ce(OEP)<sub>2</sub>]<sup>+</sup> (0.98 eV). There is a blue-shift of the B band from Ce(OEP)<sub>2</sub> to [Ce(OEP)<sub>2</sub>]<sup>+</sup>; the same trend is obtained from the calculation.

**3.2.3. YbHP<sub>2</sub>.** The experimental spectral data given in Table 8 for comparison are those measured for YbH(TPP)<sub>2</sub>.<sup>29</sup> They show three weak Q bands and a single strong B band. This is similar to Yb(OEP)<sub>2</sub>, but the protonated complex no longer has the characteristic near-IR absorption according to the calculation, in agreement with the experimental nonobservation.<sup>29</sup> The addition of an H atom to Yb(Por)<sub>2</sub> also produces a significant red-shift in the B band, as indicated by both calculation and experiment.

[Yb(TPP)<sub>2</sub>]<sup>-</sup> has a similar ground state to YbH(TPP)<sub>2</sub>, but its spectral data display significant differences.<sup>29</sup> They consist of six Q bands in addition to a single B band. These bands are assigned to the 11<sup>2</sup>E<sub>1</sub>, 13<sup>2</sup>E<sub>1</sub>, 14<sup>2</sup>E<sub>1</sub>, 17<sup>2</sup>E<sub>1</sub>, 18<sup>2</sup>E<sub>1</sub>, 20<sup>2</sup>E<sub>1</sub>, 24<sup>2</sup>E<sub>1</sub> states, respectively, according to our calculation. Also, [Yb(Por)<sub>2</sub>]<sup>-</sup> does not exhibit a strong near-IR absorption band.

#### 4. Conclusions

Even unligated YbP is nonplanar with the lanthanide atom lying considerably above the porphyrin plane. The axial ligand acac in YbP(acac) makes the metal out-of-plane displacement even larger, and it also changes the redox properties of the lanthanide monoporphyrin. The one-electron oxidation and reduction of YbP occur from the metal and porphyrin ring, respectively, but the opposite situations are found for YbP(acac). Both the first IP and EA are increased on going from YbP to YbP(acac).

The orbital energy level diagrams provide insight into the electronic structure of the lanthanide<sup>III</sup> bisporphyrin complexes. The ground-state configurations of YbP<sub>2</sub> and YbHP<sub>2</sub> are determined to be (b<sub>2</sub>/f)<sup>1</sup>(a<sub>2</sub>)<sup>1</sup> and (b<sub>2</sub>/f)<sup>1</sup>(a<sub>2</sub>)<sup>2</sup>, respectively, where b<sub>2</sub> is a metal 4f-like orbital and a<sub>2</sub> is derived from the

overlapping of the porphyrin a<sub>1u</sub> orbitals. Therefore, YbP<sub>2</sub> is a single-hole  $\pi$ -radical, similar to [Ce<sup>IV</sup>P<sub>2</sub>]<sup>+</sup>. Both one-electron oxidation and reduction of YbP<sub>2</sub> all occur from the a<sub>2</sub> orbital. The first IP is relatively small while the EA is large, which accounts for the ease of both oxidation and reduction for the porphyrin  $\pi$ - $\pi$  system. The experimental predictions of the ground states of Yb(Por)<sub>2</sub>, [Yb(Por)<sub>2</sub>]<sup>+</sup>, YbH(Por)<sub>2</sub>, [Yb(Por)<sub>2</sub>]<sup>-</sup> are supported by the calculations. The large interaction between Ln and P<sub>2</sub> accounts for the high stability of the Ln(Por)<sub>2</sub> complexes.

The calculated excitation energies and oscillator strengths are generally in good agreement with the experimental spectral data. In contrast to a normal, square planar metal porphyrin (MPor), the spectrum of a lanthanide porphyrin (whether it is a mono- or bisporphyrin) is more complicated; it contains a number of weak, low-energy absorptions to the red of the Q band. In YbP(acac), the near degeneracy of the porphyrin a<sub>1u</sub> and a<sub>2u</sub> orbitals is lifted; the a<sub>1u</sub> → LUMO and a<sub>2u</sub> → LUMO transitions become almost pure, which give rise to the Q' and Q bands, respectively. The spectrum of YbPor(acac) also exhibits two B bands, which are shown to result from a significant mixture of several transitions from lower-lying orbitals to the LUMOs. In the bisporphyrins, the strong  $\pi$ - $\pi$  interaction between the two macrocycles results in the appearance of new optical features including a number of Q bands for [YbP<sub>2</sub>]<sup>-</sup> and the strong near-IR absorption for YbP<sub>2</sub> and [CeP<sub>2</sub>]<sup>+</sup>. The origin and nature of the B bands of the bisporphyrins are also different from those of a normal MPor.

Finally, our optimized structures of the various ytterbium porphyrins in this work would aid in future X-ray crystallographic studies of corresponding compounds.

**Acknowledgment.** This work was supported by the National Institutes of Health (NIH) Grant S06 GM08047, the National Science Foundation (NSF) CREST Grant HRD0318519, and by the NSF-EPSCoR Grant NSF440900-362427-02. The ADF calculations were run on a QuantumCube QS4-2800C computer from Parallel Quantum Solutions, LLC.

**Supporting Information Available:** Cartesian coordinates of the optimized, ground-state molecular structures of the various systems, YbP, YbP(acac), YbP<sub>2</sub>, CeP<sub>2</sub>, [YbP<sub>2</sub>]<sup>+</sup>, [CeP<sub>2</sub>]<sup>+</sup>, YbHP<sub>2</sub>, and [YbP<sub>2</sub>]<sup>-</sup>, studied in this work. This material is available free of charge via the Internet at <http://pubs.acs.org>.

#### References and Notes

- (1) (a) Wong, C.-P.; Horrocks, D. W., Jr. *Tetrahedron Lett.* **1975**, 2637. (b) Buchler, J. W.; Elsässer, K.; Kihn-Botulinski, M.; Scharbert, B. *Angew. Chem., Int. Ed. Engl.* **1986**, 25, 286.
- (2) Harrison, B. S.; Foley, T. J.; Bouguettaya, M.; Boncella, J. M.; Reynolds, J. R.; Schanze, K. S.; Shim, J.; Holloway, P. H.; Padmanaban, G.; Ramakrishnan, S. *Appl. Phys. Lett.* **2001**, 79, 3770.
- (3) Foley, T. J.; Harrison, B. S.; Knefely, A. S.; Abboud, K. A.; Reynolds, J. R.; Schanze, K. S.; Boncella, J. M. *Inorg. Chem.* **2000**, 42, 5023.
- (4) Foley, T. J.; Abboud, K. A.; Boncella, J. M. *Inorg. Chem.* **2002**, 41, 1704.
- (5) He, H. S.; Wong, W.-K.; Li, K.-F.; Cheah, K.-W. *Synth. Met.* **2004**, 143, 81.
- (6) Martarano, L. A.; Wong, C.-P.; Horrocks, W. D.; Goncalves, A. M. P. *J. Phys. Chem.* **1976**, 80, 2389.
- (7) Gouterman, M.; Schumaker, C. D.; Srivastava, T. S.; Yotenani, T. *Chem. Phys. Lett.* **1976**, 40, 456.
- (8) Horrocks, W. D.; Hove, E. G. *J. Am. Chem. Soc.* **1978**, 100, 4386.
- (9) Horrocks, W. D.; Wong, C.-P. *J. Am. Chem. Soc.* **1976**, 98, 7157.
- (10) Wong, C.-P.; Venteicher, R. F.; Horrocks, W. D. *J. Am. Chem. Soc.* **1974**, 96, 7149.
- (11) Lauffer, R. B. *Chem. Rev.* **1987**, 87, 901.
- (12) Zhang, X.-B.; Guo, C.-C.; Xu, J.-B.; Shen, G.-L.; Yu, R.-Q. *Analyst* **2000**, 125, 867.

- (13) Iwase, A.; Igarashi, A. *Electrochim. Acta* **1993**, *38*, 689.
- (14) Parson, W. W.; Warshel, A. *J. Am. Chem. Soc.* **1987**, *109*, 6152.
- (15) Tran-Thai, T.-H.; Mattioli, T. A.; Chabach, D.; DeCian, A.; Weiss, R. *J. Phys. Chem.* **1994**, *98*, 8279.
- (16) Collman, J. P.; Kendall, J. L.; Chen, J. L.; Collins, K. A.; Marchon, J.-C. *Inorg. Chem.* **2000**, *39*, 1661.
- (17) Bilsel, O.; Rodriguez, J.; Milam, S. N.; Gorlin, P. A.; Girolami, G. S.; Suslick, K. S.; Holten, D. *J. Am. Chem. Soc.* **1992**, *114*, 6528.
- (18) Perng, J.-H.; Duchowski, J. K.; Bocian, D. F. *J. Phys. Chem.* **1991**, *95*, 1319.
- (19) Perng, J.-H.; Duchowski, J. K.; Bocian, D. F. *J. Phys. Chem.* **1990**, *94*, 6684.
- (20) Duchowski, J. K.; Bocian, D. F. *J. Am. Chem. Soc.* **1990**, *112*, 3312.
- (21) Donohoe, R. J.; Duchowski, J. K.; Bocian, D. F. *J. Am. Chem. Soc.* **1988**, *110*, 6119.
- (22) Buchler, J. W.; Scharbert, B. *J. Am. Chem. Soc.* **1988**, *110*, 4272.
- (23) Buchler, J. W.; deCian, A.; Fischer, J.; Kihn-Botulinski, M.; Weiss, R. *Inorg. Chem.* **1988**, *27*, 339.
- (24) Yan, X. W.; Holten, D. *J. Phys. Chem.* **1988**, *92*, 409.
- (25) Buchler, J. W.; deCian, A.; Fischer, J.; Kihn-Botulinski, M.; Paulus, H.; Weiss, R. *J. Am. Chem. Soc.* **1986**, *108*, 3652.
- (26) Dunford, C. L.; Williamson, B. E.; Krausz, E. *J. Phys. Chem. A* **2000**, *104*, 3537.
- (27) Ricciardi, G.; Rosa, A.; Baerends, E. J.; van Gisbergen, S. A. J. *J. Am. Chem. Soc.* **2002**, *124*, 12319.
- (28) Liao, M.-S.; Scheiner, S. *J. Chem. Phys.* **2002**, *116*, 3635.
- (29) Spyroulias, G. A.; Raptopoulou, C. P.; de Montauzon, D.; Mari, A.; Poilblanc, R.; Terzis, A.; Coutsolelos, A. G. *Inorg. Chem.* **1999**, *38*, 1683.
- (30) Bertini, I.; Coutsolelos, A.; Dikiy, A.; Luchinat, C.; Spyroulias, G. A.; Troganis, A. *Inorg. Chem.* **1996**, *35*, 6308.
- (31) Spyroulias, G. A.; Coutsolelos, G. A. *Inorg. Chem.* **1996**, *35*, 1382.
- (32) Spyroulias, G. A.; Coutsolelos, A. G.; Raptopoulou, C. P.; Terzis, A. *Inorg. Chem.* **1995**, *34*, 2476.
- (33) Baerends, E. J.; Ellis, D. E.; Roos, P. *Chem. Phys.* **1973**, *2*, 41.
- (34) te Velde, G.; Bickelhaupt, F. M.; van Gisbergen, S. J. A.; Fonseca-Guerra, C.; Baerends, E. J.; Snijders, J. G.; Ziegler, T. *J. Comput. Chem.* **2001**, *22*, 931.
- (35) Fonseca-Guerra, C.; Snijders, J. G.; Baerends, E. J.; te Velde, G. *Theor. Chem. Acc.* **1998**, *99*, 391.
- (36) *ADF2005.01*; SCM: Theoretical Chemistry, Vrije Universiteit, Amsterdam, The Netherlands, <http://www.scm.com>.
- (37) Vosko, S. H.; Wilk, L.; Nusair, M. *Can. J. Phys.* **1980**, *58*, 1200.
- (38) Becke, A. D. *Phys. Rev. A* **1988**, *38*, 3098.
- (39) Perdew, J. P. *Phys. Rev. B* **1986**, *33*, 8822.
- (40) Johnson, B. G.; Gill, P. M. W.; Pople, J. A. *J. Chem. Phys.* **1993**, *98*, 5612.
- (41) Li, J.; Schreckenbach, G.; Ziegler, T. *J. Am. Chem. Soc.* **1995**, *117*, 486.
- (42) Ziegler, T.; Tschinke, V.; Baerends, E. J.; Snijders, J. G.; Ravenek, W. *J. Phys. Chem.* **1989**, *93*, 3050.
- (43) Zhou, M.-F.; Andrews, L.; Ismail, N.; Marsden, C. *J. Phys. Chem. A* **2000**, *104*, 5495.
- (44) Maron, L.; Leininger, T.; Schimmelpfennig, B.; Vallet, V.; Heully, J.-L.; Teichtel, C.; Gropen, O.; Wahlgren, U. *Chem. Phys.* **1999**, *244*, 195.
- (45) van Gisbergen, S. J. A.; Snijders, J. G.; Baerends, E. J. *Comput. Phys. Commun.* **1999**, *118*, 119.
- (46) Wong, W.-K.; Zhang, L.-L.; Wong, W.-T.; Xue, F.; Mak, T. C. W. *J. Chem. Soc., Dalton Trans.* **1999**, 615.
- (47) Rosa, A.; Ricciardi, G.; Baerends, E. J.; van Gisbergen, S. J. A. *J. Phys. Chem. A* **2001**, *105*, 3311.